Report on

"Structural, Optical and Luminescent Properties of Rare Earth ion activated phosphor materials for Photonic applications"

submitted towards the partial

fulfilment of the requirements for

the award of the degree of

Master of Science

in

Physics

Submitted by

VIBHA SHARMA-2K21/MSCPHY/51

SHREYA MAURYA-2K21/MSCPHY/43

Under the supervision

of

Prof. A.S. RAO

Department of Applied Physics
DELHI TECHNOLOGICAL UNIVERSITY
(Formerly Delhi College of Engineering)
Bawana Road, Delhi-110042

May 2023

CANDIDATE'S DECLARATION

I hereby certify that the work, which is presented in the Dissertation-II entitled **"Structural, Optical and Luminescent Properties of Rare Earth activated phosphor materials for Photonic applications"** in fulfilment of the requirement for the award of the Degree of Master of Science in Physics and submitted to the Department of Applied Physics, Delhi Technological University, Delhi is an authentic record of our own, carried out during a period from January 2023 to May 2023, under the supervision of **Prof. A S Rao.**

The work presented in this report has not been submitted and not under consideration for the award for any other course/degree of this or any other Institute/University. The following works has been communicated in peer reviewed Scopus indexed conference & journal:

1. **Title of the Paper (I):** "Photoluminescence and optical studies of a temperature sustainable Dy3+ doped Silicate Phosphor for Photonic applications."

   Author(s): Vibha Sharma, Shreya Maurya, and A S Rao.

   Name of Conference: International Conference on Advanced Functional Materials and Devices (AFMD-2023)

   Date and venue: March 13-15 (2023), ARSD college-University of Delhi (Virtual mode).

   Have you registered for the conference? Yes

   Status of paper (Accepted/Published/Communicated): Accepted

   Publish in: Springer Conference Proceedings (Scopus Indexed)

   Date of paper communication: 20th April, 2023

   Date of paper acceptance: 30th May, 2023

2. **Title of the Paper (II):** "Structural, Optical and Luminescent Properties of Dy^{3+} activated KCS phosphor for white light emitting diodes."

   Author(s): Vibha Sharma, Shreya Maurya, Anu, Aman Prasad, and A S Rao.

   Journal: Luminescence (Scopus Indexed)

   Status of paper (Accepted/Published/Communicated): Communicated

   Date of paper communication: 19th April, 2023
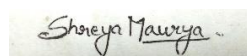
   Date of paper acceptance: --

Place: Delhi   Vibha Sharma (2K21/MSCPHY/51)

Date: 30/05/2023   Shreya Maurya (2K21/MSCPHY/43)
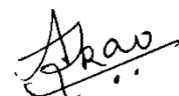
DELHI TECHNOLOGICAL UNIVERSITY

(FORMERLY Delhi College of Engineering)

Bawana Road, Delhi-110042

CERTIFICATE

I hereby certify that the project Dissertation titled "Structural, Optical and Luminescent Properties of Dy^{3+} activated KCS phosphor for white light emitting diodes" which is submitted by VIBHA SHARMA (2K21/MSCPHY/51), SHREYA MAURYA (2K21/MSCPHY/43) [Masters in Physics], Delhi Technological University, Delhi in complete fulfillment of the requirement for the award of the degree of the Master of Physics, is a record of the project work carried out by the students under my supervision. To the best of my knowledge this work has not been submitted in partition or full for any Degree or Diploma to this University or elsewhere.

Place: Delhi   (**Prof. A. S. Rao**)

Date: 30/05/2023   **SUPERVISOR**

ACKNOWLEDGEMENTS

ABSTRACT

Dysprosium (Dy^{3+}) activated potassium calcium silicate ($K_4CaSi_3O_9$) phosphor was prepared by a solid-state synthesis route. The phosphor has a cubic structure with the space group $Pa\bar{3}$ as confirmed by X-ray diffraction (XRD) measurements. Details of surface morphology and elemental composition of as-synthesized un-doped KCS phosphors were obtained by scanning electron microscopy (SEM) and energy-dispersive x-ray spectroscopy (EDS). Chemical structure as well as the vibrational modes present in the as-prepared KCS phosphors was analyzed using Fourier transform infrared spectroscopy (FT-IR). The diffuse reflectance spectra (DRS) were used to determine the optical bandgap of the phosphors and were found to be in the optical range 3.52-3.71eV. Photoluminescence (PL) spectra show intense yellow emission corresponding to the $^4F_{9/2}{\rightarrow}^6H_{13/2}$ transition under 350 nm excitation. CIE color chromaticity coordinates evaluated using the PL spectral data lie within the white region. Dexter Theory and Inokuti-Hirayama (I-H) model were applied to study the nature of energy transfer mechanism in the phosphor. Relatively high activation energy (ΔE) of the phosphors evaluated using temperature dependent PL (TD-PL) data confirms the high thermal stability of the phosphor. The above-mentioned results indicate that the as-prepared KCS:Dy^{3+} phosphor is a promising candidate for n-UV based white light emitting diodes (w-LEDs).

CONTENTS

LIST OF FIGURES

LIST OF TABLES

LIST OF ABBREVIATIONS

LED - Light-emitting diode

w-LED - White Light Emitting Diode

RE - Rare Earth (Metals)

KCS - Potassium Calcium Silicate

CCT - Correlated Color Temperature

JCPDS - Joint Committee on Powder Diffraction Standards

SEM - Scanning Electron Microscope

FWHM - Full Width at Half Maximum

CIE - Commission International De L' Eclairage

UV - Ultraviolet

PL - Photoluminescence

PLE - Photoluminescence Excitation

XRD - X-ray Diffraction

CHAPTER 1

INTRODUCTION

CHAPTER 1: INTRODUCTION

1.1 Phosphor

Phosphors have been utilized since the 19th century as a general term for materials that emit light in the absence of light. Each phosphor possesses unique characteristics, including emission colors and the duration of afterglow following excitation cessation. Electroluminescence is the phenomenon wherein phosphors emit light due to electron excitation, and these phosphors find application in the production of video displays and workstation monitors. Photoluminescence involves stimulating phosphors using UV, visible, and infrared radiation and is commonly employed in fluorescent lighting for ambient illumination. [1].
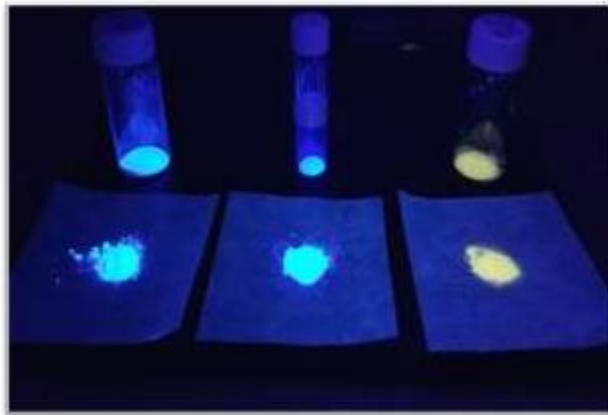
Fig. 1.1. Phosphor emitting light

Phosphors can be categorized into different groups based on the criteria used for classification, specifically focusing on chemical phosphors. Inorganic phosphors, in the form of dry powders, are the most prevalent type. Multiple synthetic methods are employed to produce these powder samples. The basic principle involves incorporating an activator ion, commonly a Rare-Earth ion, into a host matrix. Rare-earth ions are frequently used as activators in this context. [2, 3].

Phosphors consist of composites like oxide, oxynitride, sulfide, selenide, halide, borates, and oxyhalide, which are doped with small quantities of activator ions. These activator ions can be either rare-earth or transition element ions. The activator ions serve as centers for radiation or light, possessing their own distinct energy levels that can be stimulated or undergo energy transfer. [4, 5].

A phosphor's efficiency is measured by its ability to utilize excitation energy and emit light, as depicted in Fig. 1.1. To minimize afterglow, it is crucial to minimize the time delay between excitation and emission. Energy absorption can take place at the activator ion or elsewhere in the lattice, but it must ultimately be transferred to the radiating core for emission to occur [6]. The absorbed energy can also be dissipated through radiation-free processes, leading to a decrease in quantum efficiency. Effective phosphors effectively retain their ions, minimizing energy loss through non-radiative transitions. The presence of contaminant ions can absorb or redirect energy, thereby impeding the material's luminescent properties [7].

Phosphor materials are evaluated based on several crucial factors, including the range of emitting colors (such as red, green, and blue), lumen equivalency, emission spectrum, quantum yield, and emission lifespan. Color points are determined by dividing the emission spectrum energy using the Commission Internationale de l'Eclairage (CIE) graphical rule. A higher luminosity count indicates a brighter light, and phosphors should have a higher lumen equivalence. The emission spectrum of electromagnetic radiation is generated when an atom or molecule undergoes a transition from a higher to a lower energy level. It is important for phosphors to have a long emission lifespan in order to be economically viable. Quantum efficiency measures the quantity and wavelengths of emitted photons from a phosphor in relation to the number of triggering photons at specific wavelengths [8]. The decay time, also known as afterglow or persistence, refers to the time it takes for the emission intensity to decrease to 10% of its initial intensity after stimulation ceases. The decay time is determined by the intrinsic properties of the phosphormaterial[9].

Rare earth ions such as Tb^{3+}, Eu^{2+}, Dy^{3+}, Mn^{2+}, and Eu^{3+} exemplify the utilization of d-electrons in phosphors. These ions interact favorably with the crystalline host lattice through their d-orbitals. Several crucial characteristics need to be assessed to determine the suitability of synthesized phosphors for further applications. Factors such as chemical and thermal stability, quantum efficiency, color point, biodegradability, emission spectrum, and longevity play significant roles in this evaluation. Phosphor materials find applications in various technologies including plasma and field-emission displays, light-emitting diodes (LEDs), solar cells, thermal sensors, and other diverse fields. [10].

1.2 Host matrix and activator ions

Phosphors consist of a host matrix and an activator, which serves as the radiating core. Inorganic hosts possess desirable properties such as physical, thermal, and chemical inertness, making them ideal candidates. However, self-activated hosts are preferred over inorganic hosts as they exhibit their own intense and broad visible radiation when stimulated by UV light. This inherent radiation is utilized by the activator to enhance the emission intensity. [11].

The activator serves as a dopant, introduced into the crystal of the material to create the desired type of inhomogeneity. The presence of activators influences the emission delay time. The concentration of activators within the crystals is also a crucial factor to consider. While the host material is typically microcrystalline and transparent to visible light, the activators are responsible for absorbing and emitting radiation [12].

The activator plays a crucial role in collecting and amplifying the stimulating radiation, leading to an excited state. Not all ions or elements exhibit luminescence. This assessment focuses on properties such as radiation pattern, absorption spectrum, and the ratio of radiative and non-radiative transitions back to the ground state. These factors determine the ability of luminescent compounds to convert light [13].

To achieve narrow-band luminescence in the visible spectrum, rare earth elements are commonly utilized. The performance criterion for these elements is light emission, which is possible due to their unique electronic structure that allows for efficient response to high-energy stimulation such as gamma rays and X-rays. Rare-earth phosphors are often effectively excited by deep UV wavelengths.

The illuminance of trivalent rare-earth ions (Sm^{3+}, Dy^{3+} and Eu^{3+}) in silicates have recently piqued interestdue to properties such as high stability, wide UV transparency, and low composite temperature, excellent chemical and thermal stability, and high luminous efficiency [15]. Various materials like oxides, nitrates, silicates, vanadates and molybdates are used as the host but silicates are preferred as they possess high chemical and physical stability. Silicates have high temperature strength, and chemical inertness which makes them strong candidates for many practical applications.

Rare-earth ions are doped in a variety of materials are employed as activator ions for phosphor [16]. Luminescent materials activated by Dy^{3+} have gained considerable interest due to their potential applications as single-phase white light emitting phosphors. Dysprosium ions (Dy3+) exhibit at least two prominent emission bands in the blue region, ranging from 470 to 500 nm, attributed to the 4F9/2 to 6H15/2 transition and in the yellow region, spanning from 560 to 600 nm, which arise from the 4F9/2 to 6H13/2 transition. Achieving white light emission from a single-phase phosphor is highly desirable for obtaining high luminous efficiency. The selection of Dy3+ as a dopant is motivated by several factors:

1. Cost-effectiveness

2. Suitable Color Rendering Index (CRI)

3. Suitable Correlated Color Temperature (CCT)

4. Thermal and chemical stability

5. High Quantum efficiency

1.3 White light emitting diodes (w-LEDs)

A significant portion of the total energy generated across industries is used for both indoor and outdoor lighting. Typical incandescent and fluorescent lighting uses either gas discharge or heat. Due to the high temperatures involved, both phenomena are linked to significant energy losse. Along with energy efficiency, it's crucial to guarantee that the lighting technology is environmentally friendly. There is no prominent option than solid-state lighting if all of these requirements must be met. It is based on light-emitting diodes, which are essentially semiconductor chips with p-n junctions that are forward biased to emit light. Luminous efficacy, low power dissipation, persistence, environmental friendliness, and a lasting operative lifetime are just a few of the wonderful advantages that phosphor-converted light emitting diodes (pc-LEDs) have over other traditional sources of lighting [17].

The majority of currently available w-LEDs are using a blue-emitting (450-470 nm) diode, which activates a $Y_3Al_5O_{12}:Ce^{3+}$ (YAG:Ce) phosphor and causes it to generate yellow light. However, the lack of the red component in this method results in low and high CRI and CCT values respectively, in the light that is produced [18]. A common technique for producing white light is to coat an n-UV LED chip with RGB (red, green, and blue) phosphors. But it is not an easy task to maintain the proper ratio of red, blue and green colour emitting phosphors to obtain resultant white emission and use of three phosphors requires a greater number of dopants that increases the cost of LEDs.

Therefore, it is necessary to dope a single rare earth ion to lower the costs. Owing to at-least two preeminent emission bands in the blue and yellow regions, Dy^{3+} is the most assuring rare earth ion for production of white light [19]. White light produced by Dy^{3+} ions doped phosphors have high quantum efficiency, thermal stability, cost-effectiveness and desired values of CIE and CCT.

1.4 Photoluminescence (PL)

Photoluminescence refers to the emission of light by a substance after it has been exposed to light. The term "photoluminescence" is derived from the Latin word "luminescence" and the Greek suffix "photo," meaning "light." Photoluminescence occurs when a substance absorbs photons, resulting in the generation of light. This process involves the absorption of a visible-range photon by a particle, which excites an electron to a higher energy level, followed by the subsequent emission of a photon as the electron transitions to a lower-energy state. The experimental technique of photoluminescence (PL) is employed to study and characterize semiconductor nanostructures, as well as investigate their electrical properties. Photoluminescence is induced when the energy of incident photons exceeds the bandgap energy of the material. To observe photoluminescence, the wavelength of the incident light should be close to the bandgap wavelength. The PL spectrum, device temperature, and intensity, which is influenced by the irradiation intensity, provide essential data for device characterization. The photoluminescence spectrum of a semiconductor, such as GaAs, exhibits multiple distinct transitions. Therefore, the photoluminescence spectrum of GaAs becomes more complex as the material becomes purer. To analyze the photoluminescence spectrum resulting from the formation of impurities and defects, a comprehensive understanding of the energy levels is essential. Photoluminescence is a valuable characterization technique due to the extensive amount of data it offers.

Photoluminescence (PL) offers several advantages, such as rapid and easy generation of large amounts of data, indirect assessment of non-radiative recombination time, and the provision of information about energy levels and sensitivity of the system. It is a non-destructive technique used for labeling, staining, chemical marking, and revealing cosmic-ray tracks in crystals. Fluorescent lights and LEDs are widely used examples, where fluorescent coatings convert short wavelength UV (blue) light into longer wavelength (yellow) light.
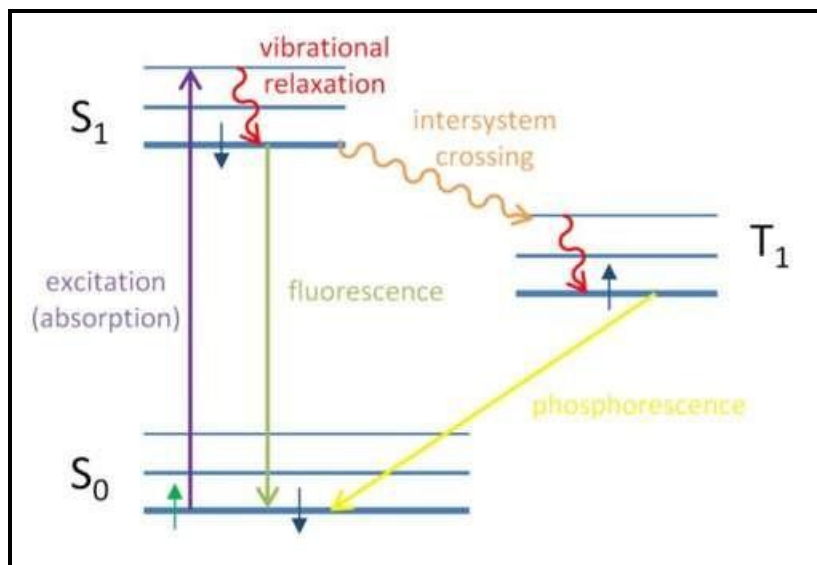
Fig. 1.2. Jablonski diagram of fluorescence and phosphorescence processes

The molecule can undergo intersystem crossover (ISC) to the excited triplet state (T1). ISC occurs when molecules possess significant spin-orbit coupling, which is often observed in heavy metals like europium and iridium due to their strong spin-orbit coupling strength. In the absence of spin-orbit coupling, the decay from the T1 state to the ground state (S0) is a forbidden transition according to angular momentum conservation, as the states have different spin multiplicities. However, the presence of spin-orbit coupling overcomes this restriction, allowing the transition from T1 to a higher-energy singlet state (S1) to occur. The transition from T1 to S0 is typically "prohibited," resulting in a long decay time, a phenomenon known as phosphorescence, as depicted in Fig. 1.2.

1.5 Fluorescence and phosphorescence

Fluorescence refers to the rapid emission of light (photoluminescence) that occurs immediately after a material has been excited by photons. On the other hand, phosphorescence refers to long-lasting photoluminescence that continues even after the excitation source has been removed. In essence, fluorescence is a type of photoluminescence that does not require a change in spin multiplicity during the radiative transition, while phosphorescence requires change in spin multiplicity during transition.

Molecules that possess paired electrons are generally stable, while those with unpaired electrons tend to be highly reactive and volatile. Electrons possess an intrinsic angular momentum known as spin, and the spin symmetry determines the possible states of an electron. When two spins are arranged in an anti-symmetric manner, the total spin is zero ($S = 0$), indicating a singlet state. Conversely, when the spins are arranged symmetrically, the total spin is one ($S = 1$), representing a triplet state. Singlet refers to the anti-symmetric arrangement of electron spin pairs with a total spin of zero, while triplet refers to the three symmetric arrangements of spin pairs with a total spin of one. When a photon is absorbed, one of the electrons in the electron pair is excited to a higher energy level, causing the molecule to be in an elevated energy state. The molecule's ground energy level is referred to as the singlet state (S0), and the photoexcited state must also be a singlet state due to the conservation of angular momentum (S1). The decay from the S1 state to the S0 state is a permissible transition (as the spin multiplicities are identical), resulting in fluorescence occurring on a time scale ranging from picoseconds to nanoseconds [20].

Fluorescence finds practical applications in various fields such as mineralogy, gemology, drug research, sensors, and the production of 3D images displayed on a monitor by directing the fluorescence at electrons. In order to tightly secure samples in a specimen container, a conductive adhesive is commonly used. When non-conductive materials are examined under the electron beam, they can accumulate charges leading to scanning defects and image errors, particularly in scanning electron (SE) imaging mode. To prevent the buildup of electrostatic charges in conventional imaging, specimens need to be good electrical conductors and have a flat surface. In the case of non-conductive samples, a thin layer of electrically conductive material is applied to cover the non-conductive components, followed by low-vacuum sputter coatings. Gold, platinum, tungsten, chromium, graphite, and other conductive materials are commonly used for specimen coatings. The scanning electron microscopy (SEM) technique is employed to investigate the morphological features, revealing micron-sized particles that are agglomerated across the entire surface [21].

CHAPTER 2

INSTRUMENTATION

CHAPTER 2: INSTRUMENTATION

2.1 X-ray diffraction (XRD)

X-ray diffraction (XRD) is a widely used and important technique for the characterization of materials. As advancements in material science technology continue to occur and new materials are being developed, there is a need to update existing analytical methods to effectively address emerging complex challenges. This allows for the exploration and resolution of intricate issues that arise in the characterization of these new materials.
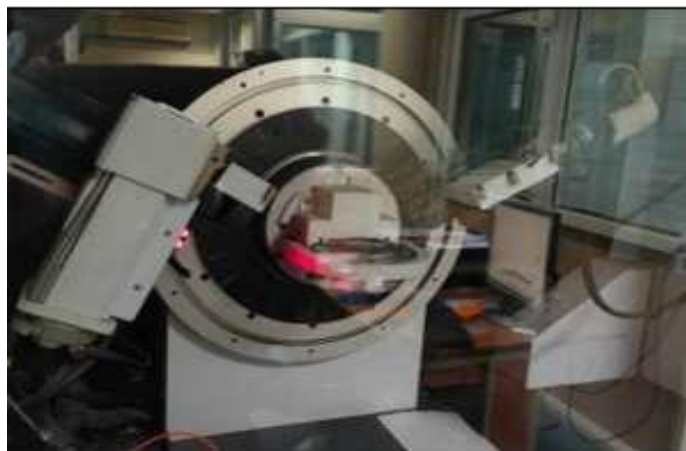
Fig. 2.2. X-ray diffraction

Despite being a well-established non-destructive technique, X-ray diffraction (XRD) still requires further advancements in its characterization capabilities, especially when dealing with complex mineral structures. This comprehensive review addresses various aspects of XRD analysis, including crystal structure determination, XRD standards, applications, potential vulnerabilities, and necessary safety precautions. The review also explores future research directions, particularly the utilization of artificial intelligence (AI) and machine learning tools, to enhance the effectiveness and accuracy of XRD analysis in mineral characterization. Topics covered include how XRD patterns can provide valuable insights into the crystalline structure, size and orientation, interplanar spacing, phase identification,

crystallite size and shape, information about lattice parameters, residual stress and strain, and thermal expansion coefficient of materials. By compiling these important discussions on XRD analysis for mineral characterization, this review aims to assist professionals and researchers in the chemical, mining, iron, metallurgy, and steel industries. This scattering process involves the dynamic interaction between X-ray photons and the atomic structure of the material. A key principle in X-ray diffraction is Bragg's law, which describes the conditions for constructive interference of scattered monochromatic X-rays. According to Bragg's law, when the scattered X-rays are in phase, they produce constructive interference, leading to the formation of diffraction patterns as shown by equation (2.1) below.

$$n\,\lambda = 2\,\sin\theta \qquad\qquad\qquad (2.1)$$

To identify an unknown substance using X-ray diffraction, a diffractometer is used to record the powder diffraction pattern. This pattern contains diffraction bands with corresponding d-values and related energies. These values are then compared to the line patterns available in Powder Diffraction File (PDF) databases, which contain information on various compounds. By matching the experimental data with the known patterns in the database, the unknown substance can be identified [22]. The value of the crystal plane spacing, denoted as d, can be estimated using the given angles between the incident beam and the perpendicular to the reflective lattice plane. By measuring the angles of each crystallographic phase, along with the degree of reflection and the wavelength of the incident beam, the spacing between the crystal planes can be calculated. This allows for the determination of the lattice parameters and provides valuable information about the crystal structure.
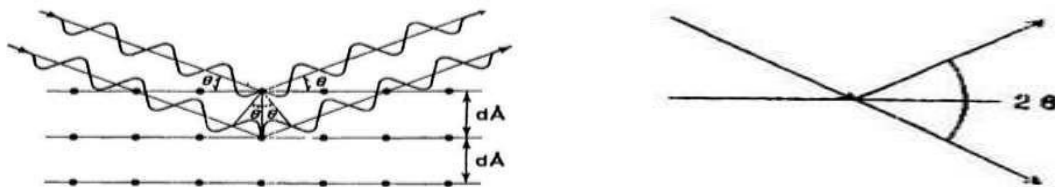
Fig. 2.3. Schematic representation of Bragg's law

To confirm the presence of a crystalline structure in a substance, whether it is a uniform material or an inhomogeneous mixture, the identification of characteristic diffraction lines is necessary. These diffraction lines correspond to specific lattice planes within the crystal structure and can be analyzed to determine the crystallographic phases present. [23].

2.1.1 Joint committee on powder diffraction standards (JCPDS)

In 1941, the Joint Committee on Powder Diffraction Standards (JCPDS) was established to maintain the Powder Diffraction File (PDF). The PDF is a database that contains information on powder X-ray diffraction patterns, including the relative intensities of prominent diffraction peaks at specific d-spacings. It is widely utilized for material classification based on X-ray diffraction patterns and is designed for various applications. Currently, it is known as the International Centre for Diffraction Data (ICDD).

The PDF, particularly the 2019 edition, consists of distinct sets of material data. Each data set includes diffraction patterns, sample requirements, research and literature data, as well as laboratory, instrumental, crystallographic, and relevant mechanical properties presented in a standardized format. The ICDD offers not only the Powder Diffraction File databases but also educational seminars, clinics, conferences, and specialized events such as the Pharmaceutical Powder X-ray Diffraction Symposium (PXRD) [24].

2.2 Diffuse reflectance spectroscopy (DRS)

Diffuse reflectance spectroscopy is a well-established technique used to analyze the spectral features of opaque solid materials. It is based on the principle that when light is incident on a substance, some of it is reflected inwardly and interacts with the material's bulk, while some of it undergoes specular reflection from the surface [25].

Fig. 2.4. Diffuse Reflectance Spectroscopy

2.3 Fourier infrared transform spectroscopy (FT-IR)

In this method, infrared light is directed through a material using a Fourier Transform Infrared (FT-IR) device. As the light passes through the material, some of it gets absorbed by the sample while the rest continues to travel through. The resulting output at the detector is a spectrum that represents the interaction of the infrared light with the sample. This spectrum typically covers a range of wavenumbers from 4000 cm-1 to 400 cm-1, and it provides valuable information about the chemical composition of the material. Each molecule has its unique spectral fingerprint, which is a characteristic pattern of absorption bands in the infrared region [26].
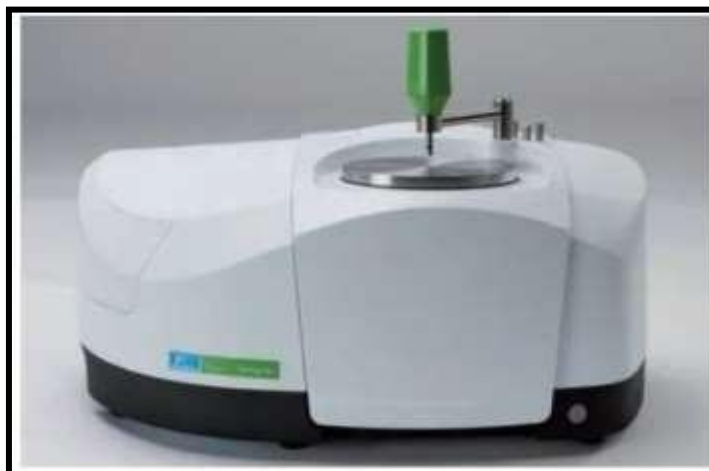
Fig. 2.5. Fourier infrared transform spectroscopy

2.4 Scanning electron microscope (SEM)

It is a technique for examining a sample's or substance's morphologies. This is due to the fact that one must first determine whether the data matches the reference, peaks, and indexes as well. After determining that the sample material has crystallized properly, the above-discussed scanning electron microscopy is carried out. The signals that are produced by the electrons' associations with the specimen's atoms include information about the specimen's structure, morphology, and crystallography as well as its surface topography and surface properties [27].

Fig. 2.6. Scanning electron microscope

In scanning electron microscopy, the electron beam uses a raster method to examine the sample. The electron source is where the electrons at the top of the column come from. When the thermal energy is more than the reference element's work function, they are released. They become activated and excited (positively charged) as a result of the anode. The entire electron column needs to be enclosed in a vacuum to protect it from noise, vibrations, and pollution. The vacuum increases the detector's ability to gather electrons while still allowing the user to see a sharp image. Lenses have control over the direction of the electrons. It employs two electromagnetic lenses: The condenser lens gathers the beam, which is subsequently transformed by the objective lens before striking the sample [28].

2.5 Photoluminescence (PL) spectroscopy

In photoluminescence spectroscopy, light is directed onto a specimen; here it is absorbed and photosensitization may take place, resulting in the emission of photoluminescence. The chromatic aberration spot width of a concentrated laser beam is of the order of 1 m for spatially resolved micro-PL at room and the lowest temperature. When scanning the sample, a CCD camera records the spectrum for each location that was looked at. Examine the emission, quantum yield, luminescence energy transfer, diffuse duration, chemical/physical durability, and other parameters while using luminous materials [29].

Fig.2.7. Photoluminescence spectroscopy

2.6 Temperature Dependent PL Spectroscopy (TDPL)

The energy levels and optical properties of materials as a function of temperature are revealed by temperature-dependent photoluminescence (PL) spectra. Researchers can learn more about the electrical transitions, carrier dynamics, and thermal effects within the material by examining how PL emission changes with temperature.

The sample is often cooled or heated over a range of temperatures while the PL spectra are taken in temperature-dependent PL measurements. As a function of temperature, the PL intensity, peak position,

and linewidth are tracked. Important properties including bandgap energy, defect states, exciton binding energies, and phonon-assisted transitions can be revealed by these values.

2.7 Time Resolved Fluorescence Spectra (TRFS)

Time-resolved fluorescence spectroscopy is a valuable technique used to investigate the decay dynamics of fluorescence emission in various materials. It provides essential information about excited-state lifetimes, fluorescence quantum yields, and interactions between fluorophores and their surroundings.

In this method, a short pulse of excitation light is employed to selectively excite the sample, and the subsequent fluorescence emission is measured at different time delays after the excitation pulse. By analysing the decay of fluorescence intensity over time, researchers can extract important parameters such as fluorescence lifetimes and identify different fluorescence decay components.


Fig.2.8. Time resolved fluorescence spectroscopy

CHAPTER 3

EXPERIMENTAL PROCEDURE

CHAPTER 3: EXPERIMENTAL PROCEDURE

3.1 Phosphor Preparation: Materials and Method

The KCS:xDy^{3+} (0.5≤x≤1.5, Δx=0.25), represented by KCSDy0.50, KCSDy0.75, KCSDy1.00, KCSDy1.25 and KCSDy1.50 respectively) were prepared using traditional solid state synthesis route. The starting materials were potassium carbonate (K_2CO_3, 99.9%), calcium carbonate ($CaCO_3$ 99.9%), silicon oxide (SiO_2 99.99%) and dysprosium oxide (Dy_2O_3 99.9%). The raw ingredients were first weighed in accordance with the nominal composition of phosphor, and then completely mixed and ground for two hours using an agate mortar and pestle. The ground samples were kept in alumina crucibles and then heated at 800° C for 5 hrs in an electric furnace. After cooling down, the final products were ground once again for further characterizations [12,13]. The complete procedure for synthesis process is represented by flowchart in Fig 2.9.
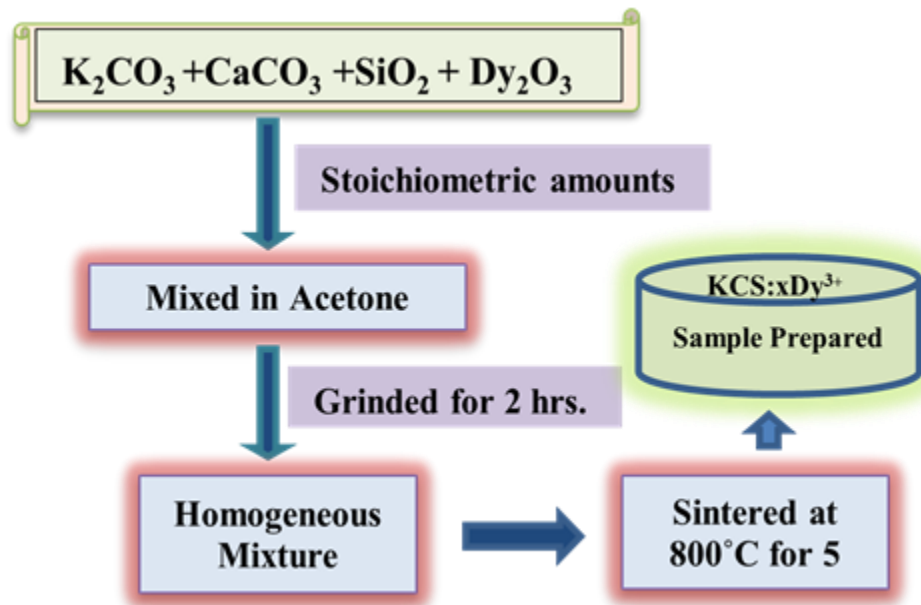
Fig.3.1. Flow chart of synthesis procedure of KCS:xDy^{3+} (0.5≤x≤1.5, Δx=0.25) phosphors.

3.2 Analysis of as-prepared sample

The crystal structures of the as-synthesised KCS:xDy^{3+} (0.5≤x≤1.5, Δx=0.25) phosphors were characterized by powder XRD analysis. The X-ray Diffraction pattern has been collected using X-ray (Bruker, model- D8 Advance) Diffractometer (Cu-Kα radiation source, λ = 1.5406 Å) and the data were obtained over the 2Ө range of 10°-60°. SEM micrographs have been recorded using JEOL 7610 F Plus machine and particle size of the as-prepared KCS phosphors was determined. FT-IR spectrum was recorded using Nicolet IS50 FT-IR instrument. The PL emission and excitation spectra were captured using a JASCO (FP-8300) Spectro fluorophotometer (1.0 nm resolution). PL lifetime decay curves were recorded by using FL3-21 TCPS instrument. Temperature-dependent Photoluminescence properties were investigated using a FLAME-S-XR1-ES spectrometer and a central heating system section.

CHAPTER 4

# RESULTS AND DISCUSSION

CHAPTER 4: RESULTS AND DISCUSSION

4.1 Structural and elemental studies

4.1.1 XRD Analysis

Fig 4.1. depicts the XRD patterns for all the Dy^{3+} ions doped KCS phosphors. The XRD patterns show complete agreement with standard data received from the Joint Committee on Powder Diffraction Standards (JCPDS) Card No. 00-039-1427. All of the as-prepared phosphor samples crystallized in single-phase cubic structure with $Pa\overline{3}$ space group. Lattice parameters of KCS phosphors were determined to be a = b = c = 15.9446 Å, V = 4053.60 Å^3 and α = β = γ = 90˚. The average crystallite size of undoped KCS phosphor has been calculated using the Debye-Scherrer equation [15]:

$$L = \frac{k\lambda}{\beta_C \cos\theta_B} \tag{1}$$

where L is the average crystallite size, k is shape factor (~0.94) and $\lambda = 1.5406$ Å is X-ray wavelength. β_c and θ are full width at half maxima and the Bragg's angle respectively. The average crystallite size for the undoped KCS phosphor sample is found to be 113.49 nm.
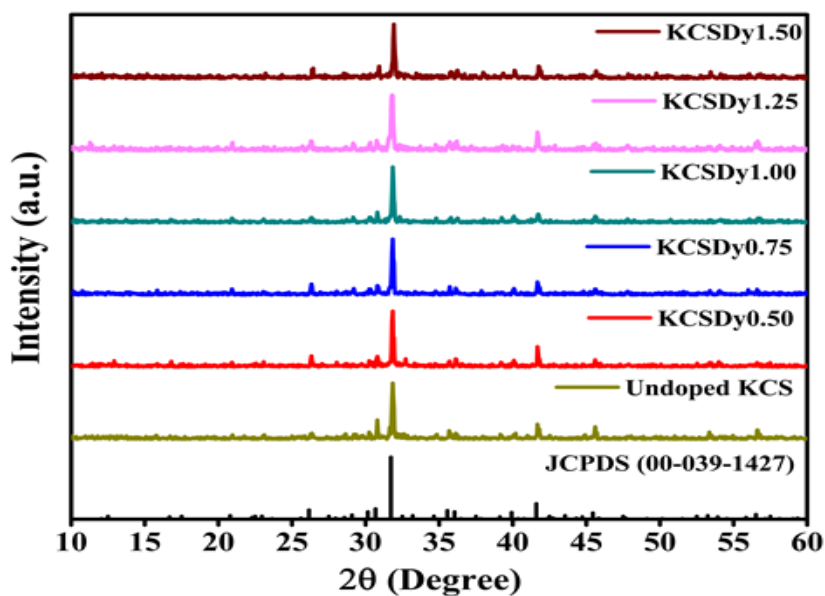

Fig.4.1. XRD of undoped and Dy^{3+} doped phosphors compared with JCPDS Card No. 00-039-1427.

Another method of calculating crystallite size is Williamson Hall (W-H) Plot. By plotting $\beta_{hkl} \cos\theta$ on y-axis against $4 \sin\theta$ on x-axis, shown in Fig. 4.2, we can evaluate the strain component from the slope and the crystallite size component from the y intercept [15]:

$$\beta_{hkl} \cos\theta_B = \frac{k\lambda}{L} + 4\,\varepsilon\,\sin\theta_B \tag{2}$$

where L, k, ε and λ represents the average crystallite size, shape factor (~0.94), strain and wavelength of X-ray (1.5406 Å), respectively. β_{hkl} and θ are full width at half maxima and the Bragg's angle, respectively. The average crystallite size for the as-prepared KCS phosphor using W-H plot approach is found to be 125.8 nm.
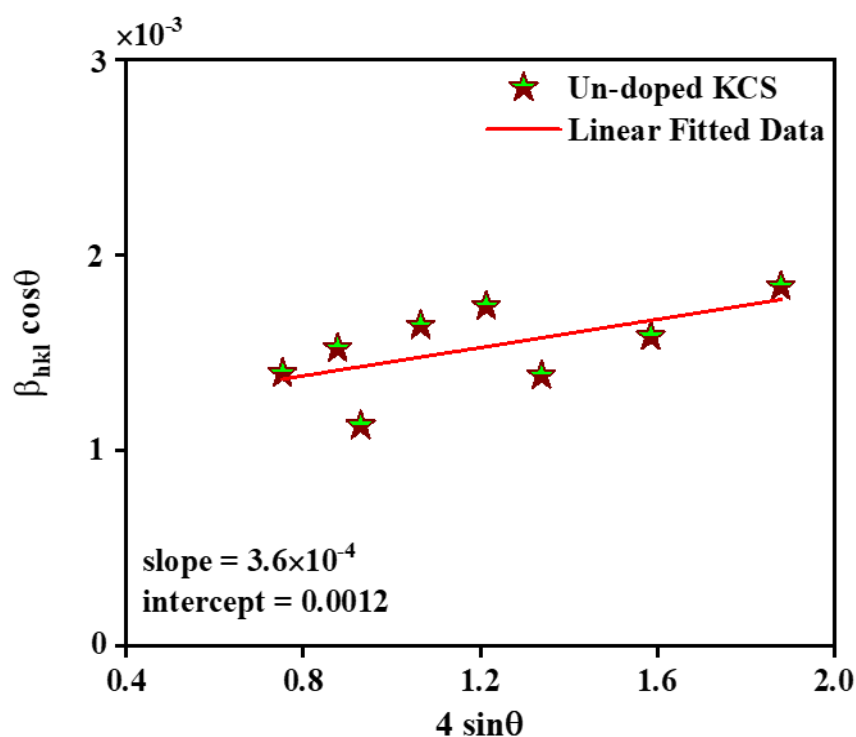

Fig.4.2. Williamson Hall Plot for undoped KCS phosphor.

4.1.2 Scanned Electron Microscopy (SEM)

The particle size is a crucial consideration from the perspective of device manufacturing. Therefore, we have described the surface shape and particle size of the KCS phosphor in this section. By employing

SEM, Fig. 4.3 depicts the surface morphology of the undoped KCS phosphor. As illustrated in Fig. 4.3a, b, and c, the SEM images were acquired at various magnifications of 0.75K, 1.3K, and 5K times. The calculated average particle size is 3.7 μm. Due to high-temperature sintering, the particles were aggregated and therefore have uneven shapes [16]. The applications of micrometer-sized crystalline particles in optoelectronic devices make them ideal for acquiring effective luminescence [17]. Fig. 4.3d shows the EDS spectrum of un-doped sample. In the EDS analysis, Ca, Si, O and K elements were present which lap up the presence of the used elements in the preparation.
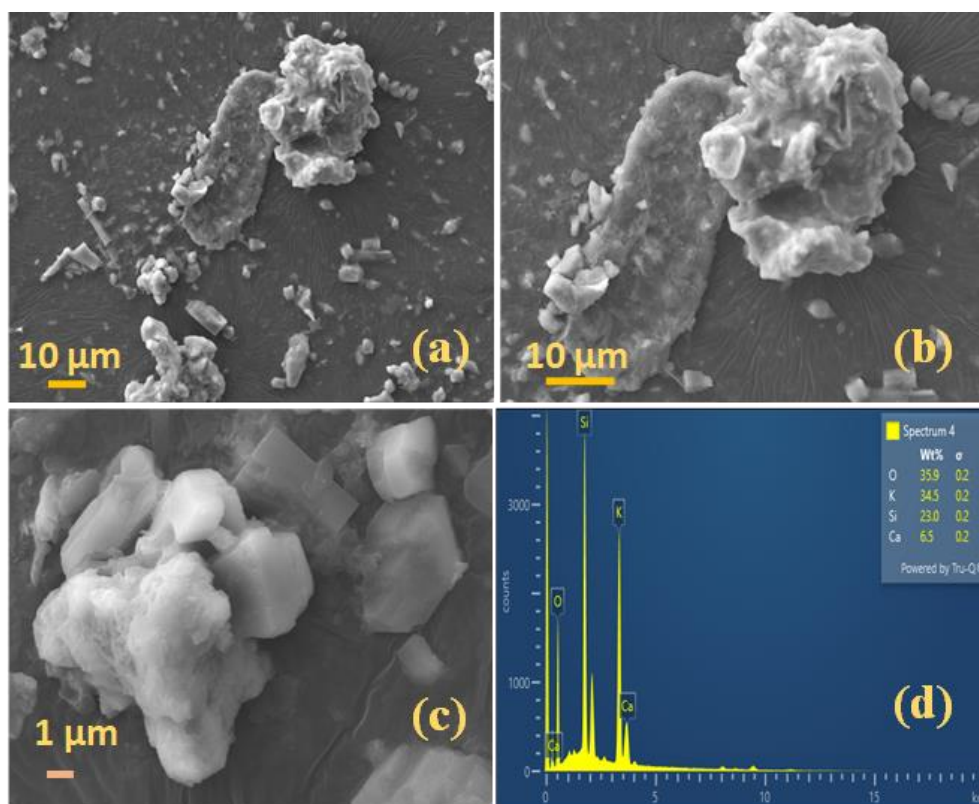
Fig.4.3. (a-c) SEM images of undoped KCS phosphor at 0.75, 1.3 and 5 KX respectively (a-c) and (d) their EDX image.

4.1.3 Fourier Transform Infrared (FT-IR) Spectrum

FT-IR is used to locate specific functional groups in molecules. A distinct set of absorption bands can be used to identify a pure compound or show the presence of particular impurities [18]. Fig. 4.4 represents the FT-IR spectrum of the undoped KCS phosphor. The major absorption bands are found in the range of wavenumbers between 450 and 1000 cm^{-1}, which is magnified in the inset of Fig. 4.4. Si-O-Si bending vibrations are responsible for the sharp peak at 477 cm^{-1} and 513 cm^{-1} [19,20]. The peaks at 663 cm^{-1} and 706 cm^{-1} conforms the Si–O–Si stretching modes for the silicate tetra-hederal.

Wavenumber (cm^{-1})	Assignment	References
477, 513, 663	Si-O-Si bending vibrations	[18, 19, 20]
706	Ca-O bending vibrations	[19]
850-1200	Asymmetric Si-O stretching modes	[21]
1387	Amide I band	[22]
1454	Ca^{2+} vibrations	[19]

Table 4.1. Bands of KCS samples corresponding to the different modes of stretching

and Ca-O bending vibrations respectively [18,19]. The absorption between (850-1200) cm^{-1} results from the asymmetric Si-O stretching modes within SiO_4 tetrahedra [21]. The peak at 1387 cm^{-1} is attributable to amide bands I [22]. Dopant Dy^{3+} ions occupy the site created by Ca^{2+} due to their corresponding ionic radii when Ca^{2+} is found in tetrahedral sites, where Ca-O bonds are eminently covalent in nature. This could lead to lattice distortion and 1454 cm^{-1} vibration modes attributed to Ca^{2+} [19].
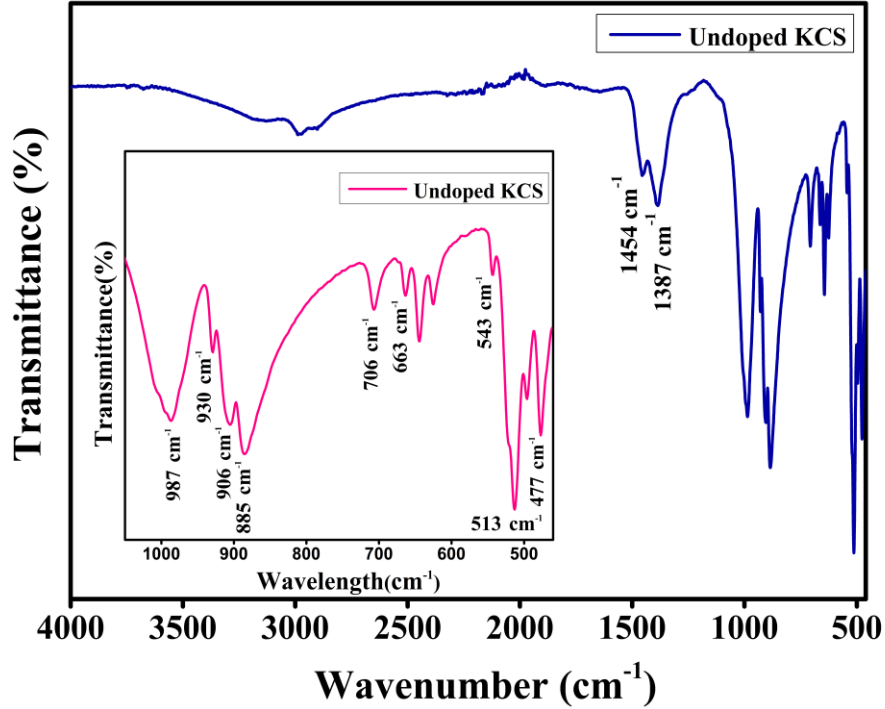
Fig.4.4. FT-IR Spectra of undoped KCS phosphor

4.2 Optical studies

4.2.1 Diffuse Reflectance Spectrum

The reflectance spectrum of 1.0 mol% doping of Dy^{3+} ions in KCS phosphor obtained in the 200-1400 nm range is shown in Fig. 4.5. The spectrum reveals a wide excitation band centred at 254 nm, which is analogous with the charge transfer between O^{2-} and Dy^{3+} ions [23] . The f-f transition of Dy^{3+} corresponds to the weak absorption peaks at 350 nm and 425 nm [23]. The transitions from the ground state of $^6H_{15/2}$ to the $^6F_{5/2}$, $^6F_{7/2}$, $^6F_{9/2}$ + $^6H_{7/2}$, and $^6F_{11/2}$ + $^6H_{9/2}$ states can be attributed to the peaks at 798 nm, 894 nm,1072 and 1268 nm of wavelengths respectively [23]. The Kubelka-Munk (K-M) theory was used to transform the reflectance data into absorption data. The K-M function is employed in order to compute the band gap of the KCS:Dy^{3+} phosphor: [24]

$$F(R) = \frac{(1-R)^2}{2R} = \frac{Q}{S}$$

(3)

Here, R represents the diffused reflectance of the sample, Q denotes the absorption coefficient and S is the scattering coefficient. The Tauc's relation correlates the band gap (E_g) and linear absorption coefficient (α) of a material:

$$\alpha h\nu = K(h\nu - E_g)^{1/2}$$

(4)

where $h\nu$ is energy of photon, E_g represents the band gap and K is a constant. By using the Eq. (3), the Tauc's relation in Eq. (4) can be modified and represented as:

$$[F(R)h\nu]^2 = C(h\nu - E_g)$$

(5)

Using the plot of $[F(R)h\nu]^2$ *versus* $h\nu$ by using the Eq. (5), the band gap value (E_g) is obtained by extrapolation of the linear fitted regions to $[F(R)h\nu]^2 = 0$. Fig. 4.5 shows the aforementioned linear fit plot of KCSDy1.0 phosphor. The values of band gap obtained from the D-R spectra using K-M function F(R) are presented in Table4.2. The inset of Fig. 4.5 shows the decreasing trend of optical band gap for the as-prepared Dy^{3+} ions doped KCS phosphor. Presence of impurities results in the formation of electron acceptor/donor levels within the bandgap which leads to the decrease in bandgap energy [25,26].

Sr. No.	Sample Name	Band Gap (eV)	τ_{avg} (ms)
1.	KCSDy0.50	3.71	1.69
2.	KSCDy0.75	3.65	1.36
3.	KCSDy1.00	3.60	1.34
4.	KCSDy1.25	3.57	1.29
5.	KCSDy1.50	3.51	1.26

**Table 4.2.** Energy band gap and lifetime values for Dy^{3+} ions doped KCS phosphors
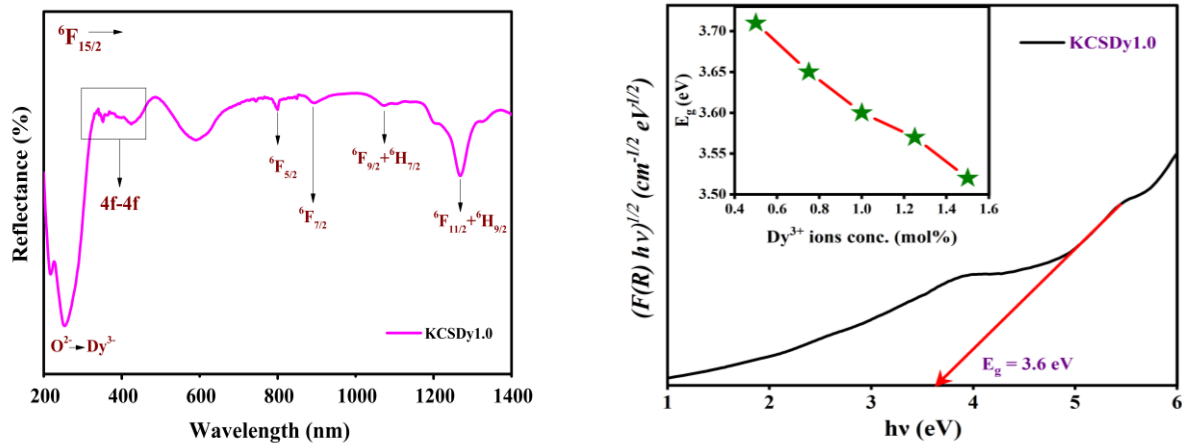
Fig.4.5. Diffused Reflectance Spectra and Energy band gap of KCSDy1.0 phosphor

4.2.2 Photoluminescence

To investigate the photoluminescent characteristics of phosphors, the excitation spectra of as-prepared Dy^{3+} doped KCS phosphors were reported and depicted in Fig.4.6. The excitation spectra were recorded in the range of 300-460 nm. The excitation spectrum consists of the $f \rightarrow f$ transitions of Dy^{3+} ions. There is a strong intense peak at 350 nm corresponding to $^{6}H_{15/2} \rightarrow {}^{6}P_{7/2}$ and relatively lower intensity peaks at 325, 338, 365, 388, 424 nm and 454 nm ascribed to the transitions from $^{6}H_{15/2} \rightarrow {}^{6}P_{3/2}$, $^{4}I_{9/2}$, $^{6}P_{5/2}$, $^{4}K_{17/2}$, $^{4}G_{11/2}$ and $^{4}I_{15/2}$, respectively. These peaks cannot be easily assured because of the dense and moderately overlapping 4f levels of Dy^{3+} in the high energy region [27]. Since the excitation band observed at 350 nm ($^{6}H_{15/2} \rightarrow {}^{6}P_{7/2}$) has highest intensity, the emission study has been prescribed by exciting all the as-prepared Dy^{3+} ions doped phosphor materials at 350 nm [27].

When the Dy^{3+} ions doped KCS phosphors were excited at 350 nm, concurrent emissions of blue (489 nm), yellow (576 nm) and a less intense red (673 nm) color were observed corresponding to $^{4}F_{9/2} \rightarrow {}^{6}H_{15/2}$, $^{4}F_{9/2} \rightarrow {}^{6}H_{13/2}$ and $^{4}F_{9/2} \rightarrow {}^{6}H_{11/2}$ transitions, respectively [28].
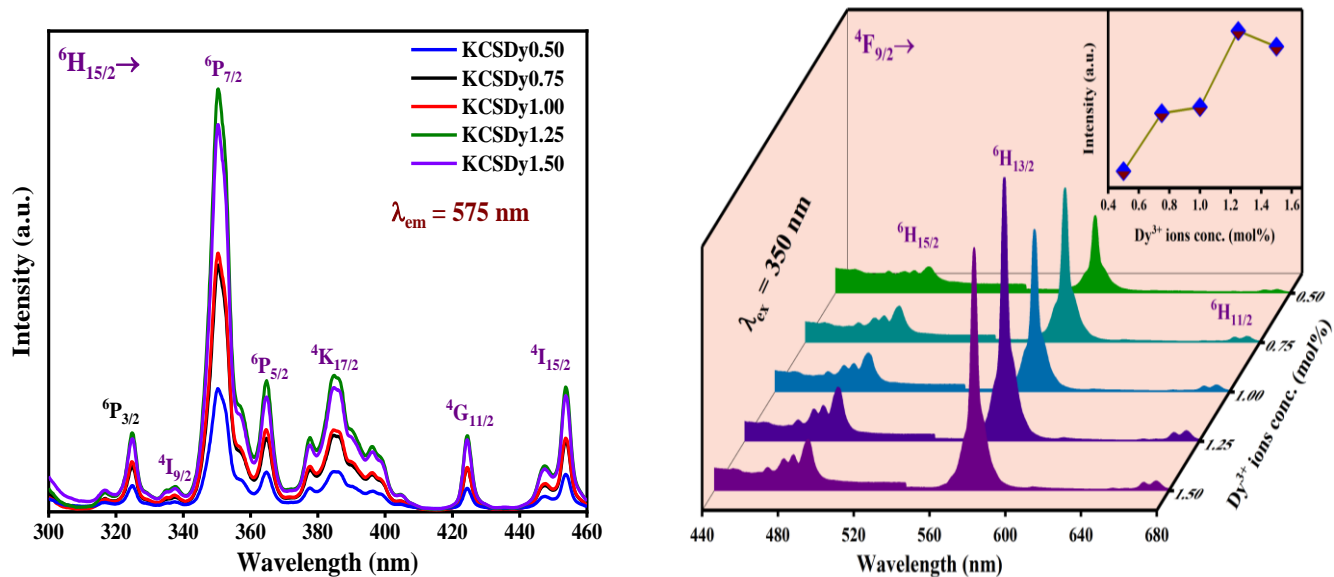
Fig.4.6. PL excitation and emission spectra of KCS:xDy^{3+} (x = 0.5, 0.75, 1.0, 1.25, 1.5) phosphors under 576 nm emission and 350 nm excitation wavelengths respectively.
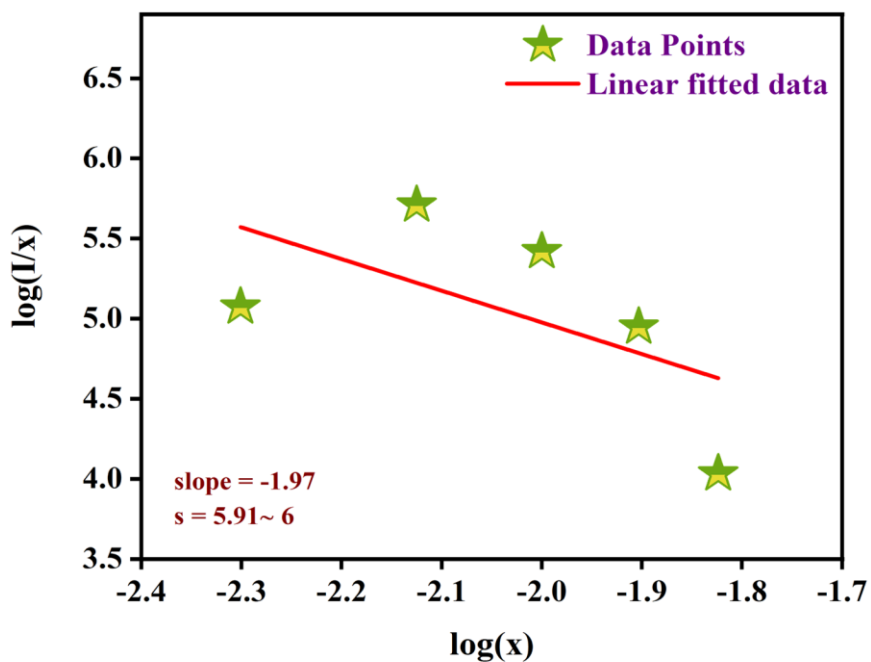
Fig.4.7. Dexter plot between log (I/x) versus log(x).

Fig. 4.6 shows the concentration influence on the PL intensities of KCS:xDy^{3+} (0.5≤x≤1.5, Δx=0.25) phosphors. As we increase the doping concentration, there was no shift in the wavelength corresponding to each peak, but the intensity starts decreasing after 1.25 mol% of Dy^{3+} ions concentration because of concentration quenching. This is primarily because Dy^{3+}-Dy^{3+} ions can transfer energy non-radiatively through exchange interactions or multipolar interactions. The following equation can be used to calculate the critical separation between Dy^{3+} ions. [29]:

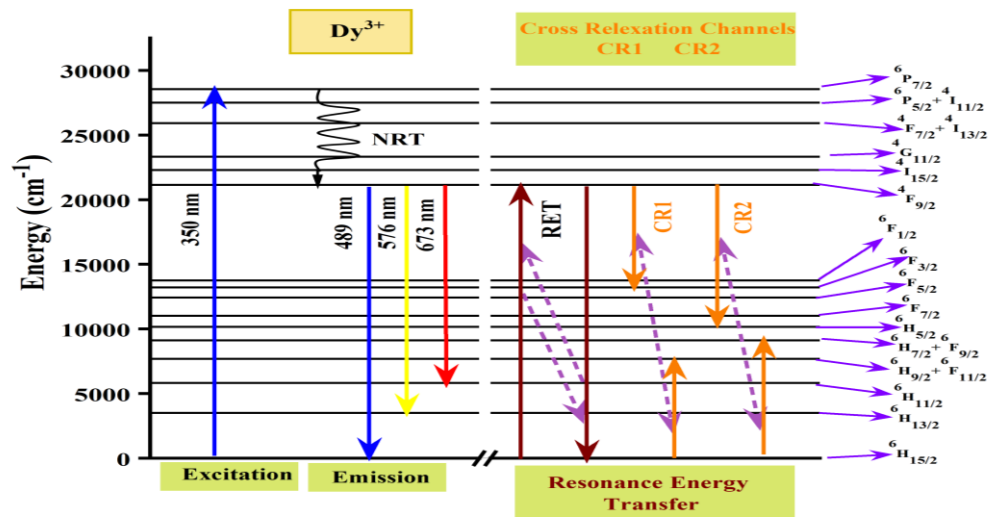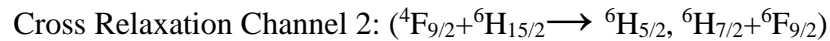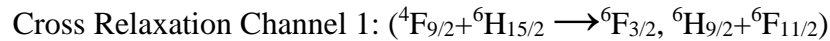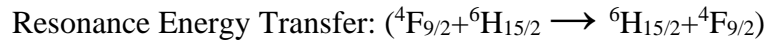$$R_C = 2\left[\frac{3V}{4\Pi X_C N}\right]^{1/3} \tag{6}$$

where R_C is the critical separation, x_C is the critical concentration, N represents the number of ions in the unit cell and V is the volume of the unit cell. For the KCS host, when N = 16, X_C = 1.25, and V = 4.0536 nm^3, the value of R_C was calculated to be 7.29 Å. It implies that the exchange interaction, which typically causes the forbidden transition with a critical distance of roughly 5 Å, will be initially excluded. [29]. Otherwise, the Dexter theory states that multipolar interaction is mostly responsible for the concentration quenching of KCS:xDy^{3+} (0.5≤x≤1.5, Δx=0.25), which can be further determined by the following equation [30]:

$$\frac{I}{c} = \frac{k}{1 + \beta(c)^{S/3}} \tag{7}$$

where c is the Dy^{3+} ions concentration, k and β are constants. S = 6, 8 and 10 indicates dipole-dipole interaction, dipole-quadrupole interaction, and quadrupole-quadrupole interaction, respectively. The plot of log(I/x) versus log(x) is perfectly linear and the value of slope is -1.96 as represented in Fig.4.7. The evaluated value of S (=5.9~6) denoting that dipole-dipole interaction is the concentration quenching mechanism of Dy^{3+} ions doped KCS phosphor.

4.2.3 Energy level diagram

The energy level diagram of the Dy^{3+} ions in as-prepared $KCS:xDy^{3+}$ ($0.5 \leq x \leq 1.5$, $\Delta x = 0.25$) phosphors is shown in Fig.4.8. The prepared phosphor material absorbs n-UV and blue light, which are associated to the absorption bands that came from $^6H_{15/2}$ to different excited energy levels of Dy^{3+} ions. The energy level diagram makes it clear that non-radiative transitions occur above $^4F_{9/2}$ level due to little energy difference between them. On the other hand, due to the substantial energy difference, radiative transition occurs from the $^4F_{9/2}$ state to the various levels $^6H_{11/2}$, $^6H_{13/2}$, and $^6H_{15/2}$. The non-radiative energy transfer and quenching may be mediated by energy transfer through resonance and cross relaxation (CR) channels between adjacent Dy^{3+} ions. The two cross relaxation channels, CR1 and CR2, and potential resonant energy transfer (RET) are given as follows when the energy match rule is taken into account [31].

Resonance Energy Transfer: ($^4F_{9/2} + {^6H_{15/2}} \longrightarrow {^6H_{15/2}} + {^4F_{9/2}}$)

Cross Relaxation Channel 1: ($^4F_{9/2} + {^6H_{15/2}} \longrightarrow {^6F_{3/2}}$, $^6H_{9/2} + {^6F_{11/2}}$)

Cross Relaxation Channel 2: ($^4F_{9/2} + {^6H_{15/2}} \longrightarrow {^6H_{5/2}}$, $^6H_{7/2} + {^6F_{9/2}}$)

Fig.4.8. Energy level diagram of Dy^{3+} ions in KCS: Dy^{3+} phosphor with excitation, emission, and cross-relaxation channels.

4.2.4 CIE chromaticity coordinates, CCT values and Colour Purity

Color coordinates are typically one of the key considerations for assessing how well phosphor renders color. PL data were used to generate the Commission International de I' Eclairage (CIE) coordinates of KCS:xDy^{3+} (0.5≤x≤1.5, Δx=0.25) phosphors under excitation wavelength of 350 nm. The color coordinates of luminous materials can be determined using the intensity-calibrated emission spectra by applying the following formula [32]:

$$x = \frac{X}{X+Y+Z} \ , y = \frac{Y}{X+Y+Z} \ , z = \frac{Z}{X+Y+Z} \tag{8}$$

Fig.4.9. shows the CIE plot for Dy^{3+} ions doped KCS phosphors. The white area contains all of the estimated CIE chromaticity coordinate values. These coordinates are very helpful in identifying a sample's precise emission color and color purity. The color purity is one of the significant variables for analysing the performance of phosphors. The following equations is used to evaluate the color purity of as-prepared Dy^{3+} ions doped KCS phosphors [33]:

$$Colour\ purity = \frac{\sqrt{(x-x_i)^2+(y-y_i)^2}}{\sqrt{(x_d-x_i)^2+(y_d-y_i)^2}} \times 100 \ \% \tag{9}$$

where (x, y) are the chromaticity coordinates of the luminescence for KCS:xDy^{3+} phosphor, (x_i, y_i) and (x_d, y_d) are the CIE coordinates for standard white light that corresponds to (1/3, 1/3) and color coordinates of dominating wavelength point respectively. Using these coordinate values, we finally obtain the color purity of KCS:xDy^{3+} (0.5≤x≤1.5, Δx=0.25) phosphors as 5.6, 7.9, 5.0, 11.0, and 7.47, respectively which is less than the earlier reported works [5,22,26]. A low color purity value suggests a clean white-light emission [5].

Another parameter is Color Correlated Temperature (CCT). The higher the CCT value, the cooler the lamp colour will appear and vice versa. Warm sources have a CCT value less than 3200K whereas cool sources have CCT values greater than 4000K. [21]. The CCT values were evaluated using the following McCamy relation [36].

$$CCT = -449\eta^3 + 3525\eta^2 - 6823.2\eta + 5520.3 \tag{10}$$

where $\eta = \frac{x-x_e}{y-y_e}$ is the inverse slope line and $(x_e = 0.3320, y_e = 0.1858)$ is epicentre. The calculated CCT values of prepared KCS:xDy^{3+} ($0.5 \leq x \leq 1.5$, $\Delta x = 0.25$) phosphors lie in the range 5672-6675 K which falls in the cool white light region. Table.4.3 summarizes the CIE parameters of Dy^{3+} doped KCS phosphor and it shows the coordinate of the emitted colour lie in the white region for all the phosphors.

Table.4.3. The CIE coordinates, CCT (K) and Colour purity (%) of as-prepared Dy^{3+} doped KCS phosphors.

Sr. No.	Sample Name	CIE coordinates		CCT (K)	Colour Purity (%)
		X	Y		
1	KCSDy0.50	0.3082	0.3393	6675	5.60
2	KCSDy0.75	0.3047	0.3289	6593	7.90
3	KCSDy1.00	0.3089	0.3338	6680	5.00
4	KCSDy1.25	0.3427	0.3654	5125	11.0
5	KCSDy1.50	0.3284	0.3515	5672	7.47
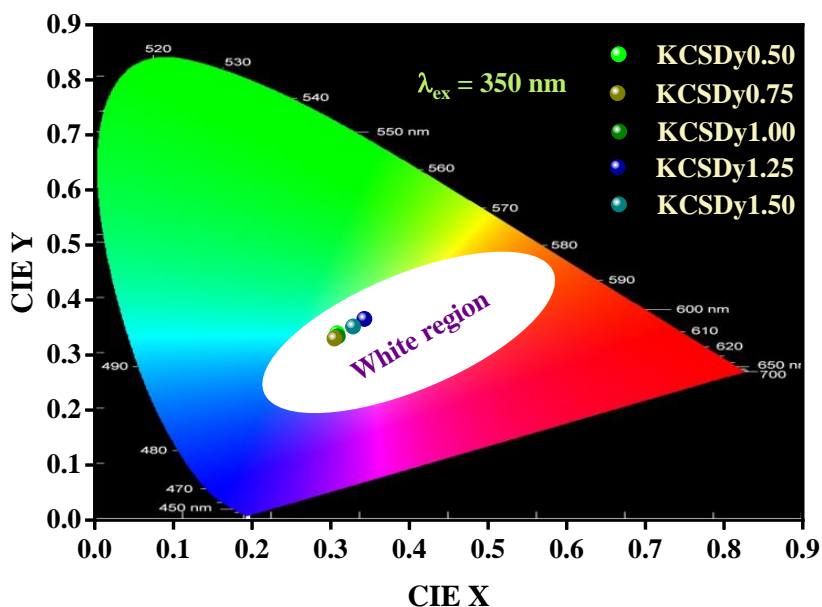
Fig.4.9. CIE chromaticity coordinates of Dy^{3+} ions in KCS:xDy^{3+} (x= 0.5, 0.75, 1.00, 1.25, 1.5) phosphors.

4.2.5 PL Decay Analysis

The fluorescence decay spectra of the phosphors are shown in Fig.4.10. The lifespan of any phosphor is crucial because it helps us determine the appropriate uses for the substance. Several exponential equations were fitted to the decay profiles, with the double exponential equation providing the perfect fit. The double-exponential fit demonstrates that energy is transferred from excited to unexcited Dy^{3+} ions, or from donor to acceptor Dy^{3+} ions, as the Dy^{3+} ion coupling becomes more prominent. The following expression can be used to calculate the PL intensity [16]:

$$I_t = I_0 + C_1 \exp\left(-\frac{t}{\tau_1}\right) + C_2 \exp\left(-\frac{t}{\tau_2}\right) \tag{11}$$

Here I_t and I_0 are the luminescence intensities at times t and 0 respectively, C_1 and C_2 are fitting constants, τ_1 and τ_2 represents fast and slow lifetimes, respectively and t is time in ms. The average decay time (τ_{avg}) for the phosphors was calculated using the following formula [32]:

$$\tau_{avg} = \frac{A_1\tau_1^2 + A_2\tau_2^2}{A_1\tau_1 + A_2\tau_2} \tag{12}$$

As a result, the corresponding Dy^{3+} lifetimes in KCS:xDy^{3+} ($0.5 \leq x \leq 1.5$, $\Delta x = 0.25$) phosphors are tabulated in Table 4.2. The lifetime decreases as the Dy^{3+} concentration increases because the ions become too close and the distance between them gradually decreases, resulting in the quenching of luminescence.

By incorporating double-exponential decay curves into the Inokuti-Hirayama (I-H) model, it is possible to investigate the energy transfer caused by ion-ion interaction in more detail. This model states that the following equation can be used to express the intensity of radiative decay as a function of time [32],

$$I(t) = I_0 \exp\left\{\frac{-t}{\tau_0} - Q\left(\frac{t}{\tau_0}\right)^{3/s}\right\} \tag{13}$$

where t and τ_0 represent the decay time after excitation and the intrinsic decay time without acceptor ions respectively and s takes up values 6, 8, or 10 representing the dipole-dipole, dipole-quadrupole, and quadrupole-quadrupole interactions, respectively. From Fig4.11, it can be seen that the decay curve for

KCSDy1.25 shows the finest fit for s = 6 in I-H model, suggesting that dipole-dipole interactions predominantly cause the double-exponential decay and therefore, energy transfers between nearby Dy^{3+} ions.
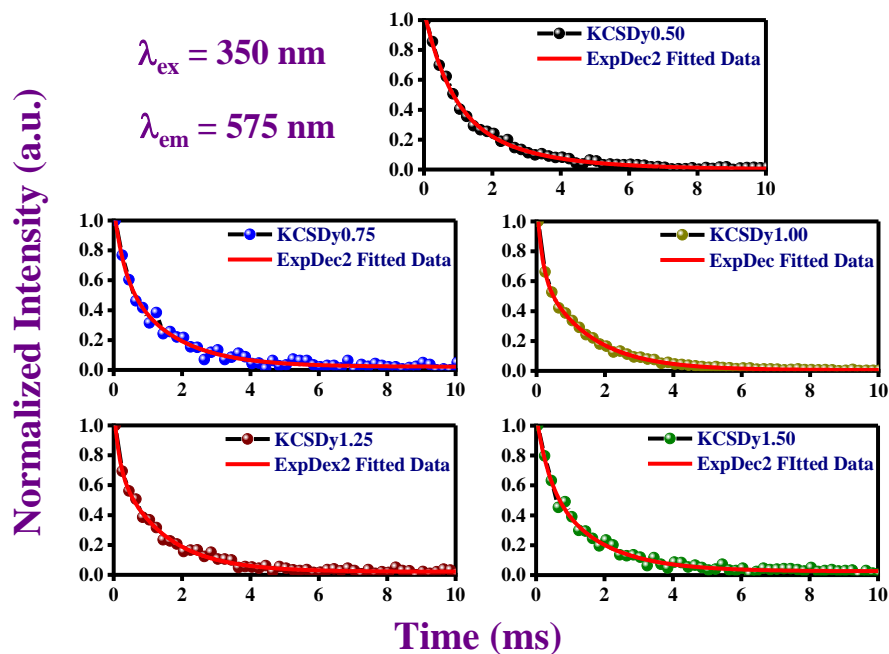
Fig.4.10. Decay spectral profiles of $^4F_{9/2} \rightarrow {}^6H_{13/2}$ transition of Dy^{3+} ions in KCS phosphors.
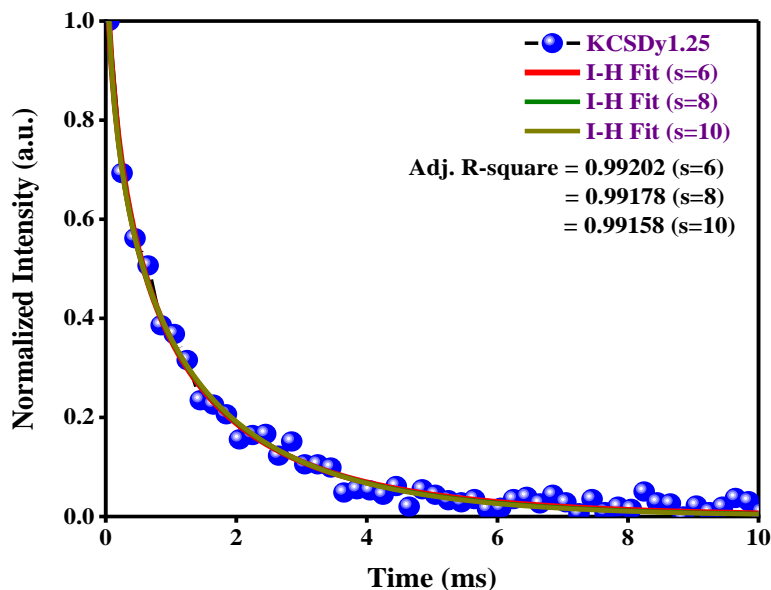

Fig.4.11. Comparison of I-H fitting (s = 6,8 and 10) for KCSDy1.25 phosphor.

### 3.2.6 Temperature dependent Photoluminescence (TD-PL)

One of the key characteristics that makes phosphor materials suitable for use in a variety of light emanating devices is the stability of luminescence with temperature. Phosphors used in lighting equipment often need strong thermal stability due to the fact that operating temperature range of UV/blue LED chips lies between 120-150 °C [39]. Hence, the TD-PL studies of the as-prepared KCSDy1.25 phosphor have been carried out under $\lambda_{ex} = 350$ nm to investigate the thermal stability in the temperature range of (18 to 170)°C. Fig.4.12 shows the variation in intensity of ${}^4F_{9/2} \rightarrow {}^6H_{13/2}$ transition by taking the initial intensity as 100% at 18 °C. The PL intensity starts decreasing with increase in temperature. At 170 °C, the as-prepared Dy^{3+} ions doped KCS phosphor retained about 64.2% of the emission intensity. The significant thermal durability of the Dy^{3+} ions doped silicate phosphor is indicated by this retaining of the PL emission intensity at 170 °C. Furthermore, the activation energy of the phosphor is calculated using Arrhenius equation [15].

$$I_t = \frac{I_0}{1 + D \exp(-\Delta E / kT)} \tag{14}$$

where k is the Boltzmann constant (8.67 10^{-5} eV K^{-1}), D is an arbitrary constant and ΔE is the activation energy. I_0 and I_t represent the intensity at 18 °C and any temperature T(°C), respectively. In order to calculate ΔE, the value of slope is calculated by plotting $\ln[(I_0/I_T)-1]$ versus $1/k_BT$ (as shown in Fig.4.13). ΔE is equal to 0.30 eV for as-synthesized Dy^{3+} phosphors, which is greater than the values found in earlier investigations for $Ca_3Bi (PO_4)_3:Dy^{3+}$ (0.223 eV) [31] and BZPO: Ce^{3+}, Dy^{3+}/Tb^{3+} phosphors (0.15 eV) [32]. Comparatively high value of ΔE indicates their thermal stability and supports their prospective use in SSL devices [29].
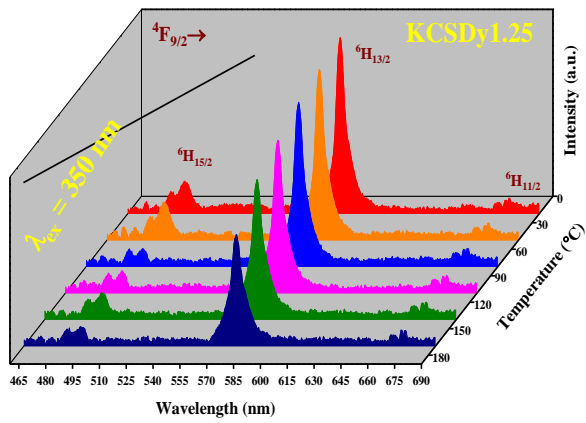
Fig.4.12. TDPL spectra of KCSDy1.25 phosphor.
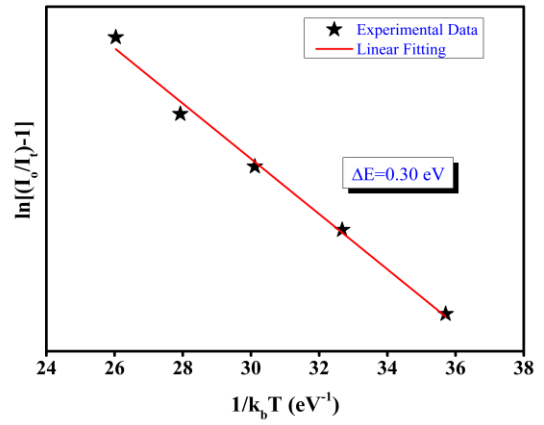
Fig.4.13. Plot between $\ln[(I_0/I_T)-1]$ versus $1/K_BT$.

CHAPTER 5

CONCLUSION

CHAPTER 5: CONCLUSIONS

In the present work, a series of Dy^{3+} doped KCS phosphors was prepared using conventional solid state reaction method and analysed for their structural, morphological and optical properties using XRD, SEM, FT-IR, DRS, PL, luminescence decay and TD-PL studies. The phase purity and the cubic structure are exhibited through XRD analysis. Morphological studies reveals that the particle size of phosphors lie in micrometre range and EDS data demonstrates the existence of all the constituent elements employed in the synthesis process of the phosphors. The existence of various bands in the FT-IR spectrum indicates the presence of distinct molecular bonds in the host matrix. Indirect band gaps for the whole series were evaluated using Tauc's Plot. In PL spectra under excitation of 350 nm, a relatively high intensity peak is obtained at 576 nm. The optimum doping concentration is found to be 1.25% after which concentration quenching occurs. The dipole-dipole (s = 6) interaction was found to be the most prevalent energy transfer mechanism causing the quenching using the Dexter theory and I-H model. The CIE coordinates for all Dy^{3+} ions doped KCS phosphors lie within the white region. According to decay profiles for the $^4F_{9/2} \rightarrow {}^6H_{13/2}$ transition at λ_{ex} = 350 nm, the experimental lifetime values for as-prepared phosphors decrease as the concentration of Dy^{3+} ions rises. Furthermore, according to TDPL characteristics, the intensity retention was around 64.2% at 443 K and a relatively high activation energy of 0.30 eV was obtained, demonstrating the phosphor's good thermal stability. All of the aforementioned findings enable us to conclude the suitability of the as-prepared Dy^{3+} doped KCS phosphors for their application in w-LEDs excited by n-UV light.

CHAPTER 6

SCOPE OF WORK

CHAPTER 6: SCOPE OF WORK

The recent work has been done by doping Dysprosium (Dy^{3+}) into KCS host material which have made them an effective and high-quality phosphor which can be used in low-cost developed phosphor-converted white light-emitting diodes (pc-w-LEDs). Firstly, the luminescent properties of thesephosphor can be enhanced via co-doping with other suitable rare-earth ions (RE) such as yttrium (Y^{3+}), samarium (Sm^{3+}), gadolinium (Gd^{3+}), terbium (Tb^{3+}), and lutetium (Lu^{3+}), etc. This is because RE ions co-doped in specific regions of host matrix could enable a new generation of quantum integrated photonicdevices.

The present phosphor has been synthesized by the conventional solid-state reaction technique and characterized for their structural and photoluminescence properties. So, another synthesis method such as sol-gel method can be explored to improve the particle morphology and reduce the particle size. The sol-gel combustion method employs a hybrid of the sol-gel and combustion processes, with nitrates as metal precursors. The metal oxides that are generated go through numerous processes in the Sol–gel approach. First, the metal nitrate is rapidly hydrolyzed; second, the metal hydroxide solution is condensed to create gels; and finally, xerogel is formed following the evaporation process, which is then combusted at a high temperature. The resulting compound is a black fluffy structure that is sintered at various temperatures. This method may be explored to improve the luminescence properties of the as-prepared phosphor.

The utility of these phosphor can not only be applied for w-LEDs but also is extended for versatile applications such as fingerprint sensing and thermal sensing, bio-imaging, etc. In a nutshell, the prototype w-LEDs can be fabricated using the optimized phosphor for the above-mentioned applications.

REFERENCES

[1] S. Pradhan, H. Kaur, M. Jayasimhadri, Photoluminescence and thermal sensing properties of Er^{3+} doped silicate-based phosphor for multifunctional optoelectronic device applications, Ceram. Int. 47 (2021) 27694–27701.

[2] Z. Li, X. Geng, Y. Wang, Y. Chen, Synthesis and luminescence properties of $NaBaPO_4$:Tm^{3+}, Dy^{3+} white-light emitting phosphor with enhanced brightness by Li^+ co-doping, J. Lumin. 240 (2021).

[3] G.R. Dillip, G.B. Kumar, V.R. Bandi, M. Hareesh, B. Deva Prasad Raju, S.W. Joo, L.K. Bharat, J.S. Yu, Versatile host-sensitized white light emission in a single-component $K_3ZnB_5O_{10}$: Dy^{3+} phosphor for ultraviolet converted light-emitting diodes, J. Alloys Compd. 699 (2017) 1108–1117.

[4] T.S. Sreena, P.P. Rao, A.K.V. Raj, T.R.A. Thara, Narrow-band red-emitting phosphor, $Gd_3Zn_2Nb_3O_{14}$: Eu^{3+} with high color purity for phosphor-converted white light emitting diodes, J. Alloys Compd. 751 (2018) 148–158.

[5] H. Kaur, M. Jayasimhadri, Color tunable photoluminescence properties in Eu^{3+} doped calcium bismuth vanadate phosphor for luminescent devices, Ceram. Int. 45 (2019) 15385–15393.

[6] Q. Zhang, X. Wang, Y. Wang, Design of a broadband cyan-emitting phosphor with robust thermal stability for high-power WLED application J. Alloys Compd. 886 (2021) 161217.

[7] L. Jun, X. Shuping, G. Shiyang, FT-IR and Raman spectroscopic study of hydrated borates, Spectrochim. Acta A Mol. Biomol. Spectrosc. SPECTROCHIM ACTA A. 51 (1995) 519-532.

[8] C.S. Lim, A.S. Aleksandrovsky, M.S. Molokeev, A.S. Oreshonkov, D.A. Ikonnikov, V. v. Atuchin, Triple molybdate scheelite-type upconversion phosphor $NaCaLa(MoO_4)_3$:Er^{3+}/Yb^{3+}: Structural and spectroscopic properties, Dalton Trans. 45 (2016) 15541–15551.

[9]   S. Das, A. Amarnath Reddy, S. Surendra Babu, G. Vijaya Prakash, Controllable white light emission from Dy^{3+}-Eu^{3+} co-doped $KCaBO_3$ phosphor, J. Mater. Sci. 46 (2011) 7770–7775.

[10]   B. Han, Y. Dai, J. Zhang, B. Liu, H. Shi, Development of near-ultraviolet-excitable single-phase white-light-emitting phosphor $KBaY(BO_3)_2$:Ce^{3+}, Dy^{3+} for phosphor-converted white light-emitting-diodes, Ceram. Int. 44 (2018) 14803–14810.

[11]   M. Jayachandiran, S.M.M. Kennedy, Synthesis and optical properties of $Ba_3Bi_2(PO_4)_4$: Dy^{3+} phosphor for white light emitting diodes, Journal of Alloys and Compounds. 775 (2019) 353–359.

[12]   Y. Shi, Z. Yang, W. Wang, G. Zhu, Y. Wang, Novel red phosphor Na_2CaSiO_4:Eu^{3+} for light-emitting diodes, Mater. Res. Bull. 46 (2011) 1148–1150.

[13]   X. Lei, G. Li, M. Zeng, B. Zhou, Z. Yuan, Y. Hu, H. Gu, Y. Li, W. Chen, Europium-doped $NaBaB_9O_{15}$ phosphor with controllable blue/red dual-band emissions through self-reduction for plant growth LEDs, J. Lumin. 237 (2021) 118166.

[14]   C.H. Lin, C.H. Huang, Y.M. Pai, C.F. Lee, C.C. Lin, C.W. Sun, C.H. Chen, C.W. Sher, H.C. Kuo, Novel method for estimating phosphor conversion efficiency of light-emitting diodes, Crystals (Basel). 8 (2018) 120442.

[15]   H. Kaur, M. Jayasimhadri, Spectroscopic and color tunable studies in Dy^{3+}/Eu^{3+}co-doped calcium-bismuth-vanadate phosphor for lighting applications, Solid State Sci. 122 (2021) 106776.

[16]   M. Sahu, N. Phatak, M.K. Saxena, Exploring color tunable emission characteristics of Eu^{3+}-doped $La_2(MoO_4)_3$ phosphor in the glass-ceramic form, RSC Adv. 11 (2021) 17488–17497.

[17]   L. Wang, X. Guo, Q. Song, J. Li, X. Wang, N. Wang, Y. Li, Y. Han, G. Jia, Multicolor barium molybdate phosphor doped with Re^{3+} (Re = Eu, Sm, Tb, Dy) via solid-state method: Synthesis and characterizations, Modern Physics Letters B. 32 (2018).

[18]   T. Sakthivel, G. Annadurai, R. Vijayakumar, X. Huang, Synthesis, luminescence properties and thermal stability of Eu^{3+}- activated $Na_2Y_2B_2O_7$ red phosphor excited by near-UV light for pc-WLEDs, J. Lumin. 205 (2019) 129–135.

[19]   C. Dou, Z. Wang, Y. Yin, C. Liu, F. Zheng, S. Sun, B. Teng, J. Li, D. Zhong, Realization of non-rare earth doped blue-emitting phosphor $Ba_2Y_5B_5O_{17}$: Sb by selective site excitation, and its application in n-UV excited wLEDs, J. Lumin. 239 (2021) 118326.

[20]   J. Grigorjevaite, A. Katelnikovas, Synthesis and optical properties investigation of blue-excitable red-emitting $K_2Bi(PO_4)(MoO_4)$:Pr^{3+} powders, J. Mater. Res. Technol. 9 (2020) 15779–15787.

[21]   Y. Zhai, W. Zhang, Y. Yin, J. Wang, C. Hu, X. Li, Facile hydrothermal synthesis and luminescent properties of monodisperse ellipsoid-like $NaLa(MoO_4)_2$:Sm^{3+} red-emitting phosphor, J. Mater. Sci.: Mater. Electron. 27 (2016) 9690–9698.

[22]   B. Valeur, M.N. Berberan-Santos, A brief history of fluorescence and phosphorescence before the emergence of quantum theory, J. Chem. Educ. 88 (2011) 731–738.

[23]   Fluorescence and Phosphorescence - Chemistry LibreTexts, (n.d.).

[24]   P. Basu, Analytical techniques, Biomass Gasification, Pyrolysis and Torrefaction: Practical Design and Theory. (2018) 479–495.

[25]   F. Sima, C. Ristoscu, L. Duta, O. Gallet, K. Anselme, I.N. Mihailescu, Laser thin films deposition and characterization for biomedical applications, Laser Surface Modification of Biomaterials: Techniques and Applications. (2016) 77–125

[26]   N. Fleck, H. Amli, V. Dhanak, W. Ahmed, Characterization techniques in energy generation and storage, Emerging Nanotechnologies for Renewable Energy. (2021) 259–285.

[27] R. Jenkins, T.G. Fawcett, D.K. Smith, J.W. Visser, M.C. Morris, L.K. Frevel, JCPDS — International Centre for Diffraction Data Sample Preparation Methods in X-Ray Powder Diffraction, Powder Diffraction. 1 (1986) 51–63.

[28] A.J. Moy, J.W. Tunnell, Diffuse Reflectance Spectroscopy and Imaging, Imaging in Dermatology. (2016) 203–215.

[29] N.R.R. Anbusagar, K. Palanikumar, A. Ponshanmugakumar, Preparation and properties of nanopolymer advanced composites: A review, Polymer-Based Nanocomposites for Energy and Environmental Applications: A Volume in Woodhead Publishing Series in Composites Science and Engineering. (2018) 28–73.

[30] N.C.I.S. Furuvik, L. Wang, R. Jaiswal, R. Thapa, M.S. Eikeland, B.M.E. Moldestad, Experimental study and SEM-EDS analysis of agglomerates from gasification of biomass in fluidized beds, Energy. 252 (2022) 124034.

[31] L. Gómez, I. Martínez, M. v. Navarro, T. García, R. Murillo, Sorption-enhanced CO and CO_2 methanation (SEM) for the production of high purity methane, Chem. Eng. J. 440 (2022) 135842.

[32] The Current Situation in Ultra-Precision Technology – Silicon Single Crystals as an Example, Advances in CMP Polishing Technologies. (2012) 15–111.

PLAGIARISM REPORT

turnitin

PAPER NAME

VIBHA & SHREYA M.Sc Thesis (2).docx

WORD COUNT

6792 Words

CHARACTER COUNT

38445 Characters

PAGE COUNT

27 Pages

FILE SIZE

82.7KB

SUBMISSION DATE

May 30, 2023 1:18 PM GMT+5:30

REPORT DATE

May 30, 2023 1:19 PM GMT+5:30

● 20% Overall Similarity

The combined total of all matches, including overlapping sources, for each database.

- 10% Internet database
- Crossref database
- 15% Submitted Works database

- 12% Publications database
- Crossref Posted Content database

● Excluded from Similarity Report

- Bibliographic material

- Small Matches (Less then 8 words)

Vibha Sharma – 2K21MSCPHY51

Shreya Maurya – 2K21MSCPHY43

(**Prof. A. S. Rao**)

STUDENTS   **SUPERVISOR**

ACCEPTANCE PROOF

ARSD afmd 12:02 AM

to me ∧

↩ ⋮

From ARSD afmd · afmd2023@arsd.du.ac.in

To Vibha · vibha78600@gmail.com

Date 30 May 2023, 12:02 AM

🔒 Standard encryption (TLS).
See security details

Dear Ms. Sharma

I am pleased to inform you that your manuscript entitled **"Photoluminescence and optical studies of a temperature sustainable Dy3+ doped Silicate Phosphor for Photonic applications"** has been accepted for publication in Advanced Functional Materials Devices (AFMD-2023) proceedings.

Thank You

Convener
AFMD-2023

Show quoted text

M Gmail

Vibha <vibha78600@gmail.com>

2nd International Conference on "Advanced Functional Materials and Devices"(AFMD-2023)

Google Forms <forms-receipts-noreply@google.com>   Fri, Feb 10, 2023 at 11:58 AM
To: vibha78600@gmail.com

Thanks for filling out 2nd International Conference on "Advanced Functional Materials and Devices"(AFMD-2023)

Here's what was received.

2nd International Conference on "Advanced Functional Materials and Devices"(AFMD-2023)

AFMD 2023 to be held via Online Mode from 13th to 15th March 2023
Selected papers will be published in Springer Proceedings

Early Bird Registration fee
For Student: Rs. 500/- (Indian)/ $ 50 (Foreign)
For Academician/Researcher: Rs. 1000/- (Indian)/ $75 (Foreign)

Payment must be made online through Net banking/NEFT
Bank Details:
Name: Atma Ram Sanatan Dharma College
Bank Name: ICICI Bank
A/c No. 017101020425
IFSC: ICIC0000171
Branch: Saket, New Delhi

No files submitted

Payment Information *

◉ Paid

○ Unpaid (If registering later than email your receipt/ transaction proof at
afmd2023@arsd.du.ac.in)

If Paid then upload transaction proof/receipt

Submitted files

📷 Receipt - Vibha.jpg

Transaction ID

IMPS00222886508

Create your own Google Form
Report Abuse

SCOPUS INDEXING PROOF

AFMD-2023 Invitation

After the successful completion of AFMD-2021, it gives us immense pleasure to invite you to attend the 2nd International conference on Advanced Functional Materials and Devices (AFMD-2023) to be organized online during March 13-15, 2023. This conference is being organized in succession with previous event held in March 2021. The principal motive of AFMD-2023 is to provide a common platform for all the researchers, academic personnel's, scientist, research students from all over the world to brainstorm, discuss and share their new achievements, ideas, results and new innovations regarding new functional materials for device purposes.

Technical Sessions: The symposium will comprise of plenary, invited and contributed papers. Contributed papers will be presented orally as well as during poster session covering recent developments in the areas listed above.

Presentations: Keynote lectures will be of 45 minutes duration. Duration of invited talk and oral presentation will be 30 mins. and 15 mins. respectively.

Publications: Abstract book will be published. Selected peer reviewed papers will be published in Scopus / Web of science indexed International journal/ Book Proceedings of repute.

Scope of symposium

(Not limited to the following):
- Sensors, Transducer, flexible electronics
- Fuel cells, solar cells and energy storage devices
- Materials for Energy Harvesting Applications
- Bulk and composite materials
- Materials for Biomedical Applications
- Systems for Environmental studies
- Applications of Carbon Nanomaterials
- Materials for Photonics and Optoelectronics
- Applications of Magnetic Materials
- Materials with Multifunctional Properties
- Theoretical methods for nanomaterials and nanotechnology
- Physics and application of heterostructures and superlattices
- Biocompatible systems for medical applications
- Advanced materials for Military applications
- High energy and particle physics

Submit abstract @
https://forms.gle/aVN8Xn3QkkcnUHGp6

Important Dates

Abstract Submission Opens: Dec 10, 2022

Abstract Submission Ends: Feb 10, 2023

Acceptance Notification: Feb 20, 2023

Registration Opens: Jan 01, 2023

Conference Commences: March 13, 2023

Registration

Category	Early bird registration (Before 01/03/2023)		After 01/03/2023	
	Indian (INR)	Foreign (USD)	Indian (INR)	Foreign (USD)
Academician/ Researcher	1000	75	1500	100
Students	500	50	750	75

Organizers

Chief Patron
Shri Pawan Jaggi
Chairman, College Governing Body
Patron
Prof. Gyantosh Kr. Jha (Principal)
Conference Chair
Dr. Vinita Tuli (Coordinator, IQAC)
Convener and Program Chair
Dr. Shankar Subramanian
Dr. Anjali Sharma
Conference Secretaries
Dr. Raghvendra Pandey
Dr. Anjani Kumar Singh
Dr. Manisha
Mr. Md. Sadiq
Dr. Amit Vishwakarma
Dr. Abid Hussain

Contact us

Secretariat Office
Atma Ram Sanatan Dharma College
University of Delhi,
Dhuala Kaun, Delhi-110021, India
Email: afmd2023@arsd.du.ac.in
Web: https://conference.arsdcollege.ac.in/AFMD2023/Home.htm
Ph: +91 9540794900; +91-9811685798